Open access • Journal Article • DOI:10.1029/2004JA010804

High-altitude cusp flow dependence on IMF orientation: A 3-year Cluster statistical study — Source link

Benoit Lavraud, Andrei Fedorov, E. Budnik, Michelle F. Thomsen ...+6 more authors

Institutions: Los Alamos National Laboratory, Swedish Institute of Space Physics, Imperial College London, Rutherford Appleton Laboratory

Published on: 01 Feb 2005 - Journal of Geophysical Research (John Wiley & Sons, Ltd)

Topics: Magnetopause, Magnetosheath, Interplanetary magnetic field, Plasma sheet and Magnetic reconnection

High-altitude cusp flow dependence on IMF orientation: A 3-year Cluster statistical study

B. Lavraud, A. Fedorov, E. Budnik, M. F. Thomsen, A. Grigoriev, P. J. Cargill, M. W. Dunlop, H. Rème, J. Dandouras, A. Balogh

High-altitude cusp flow dependence on IMF orientation: A 3-year Cluster statistical study

B. Lavraud,[1] A. Fedorov,[2] E. Budnik,[2] M. F. Thomsen,[1] A. Grigoriev,[3] P. J. Cargill,[4] M. W. Dunlop,[5] H. Rème,[2] I. Dandouras,[2] and A. Balogh[4]

Received 24 September 2004; revised 9 November 2004; accepted 1 December 2004; published 15 February 2005.

[1] We report on the statistical properties of the plasma flows measured by the Cluster spacecraft in the high-altitude cusp region of the Northern Hemisphere as a function of the interplanetary magnetic field (IMF) orientation, with selected clock angle intervals. The technique uses a magnetic field model, taking into account the actual solar wind conditions and level of geomagnetic activity, in order to model the magnetopause and cusp displacements as a function of these conditions. The distributions of the magnetic field vector show a clear consistency with the IMF clock angle intervals chosen and demonstrate that the technique used here fixes the positions of the cusp boundaries adequately. The antisunward convection observed in the exterior cusp suggests that this region is statistically quite convective under southward IMF, while for northward IMF the region appears more stagnant. The presence of large parallel (downward) flows at the equatorward edge of the cusp shows that plasma penetration occurs preferentially at the dayside low-latitude magnetopause for southward IMF conditions; in contrast, under northward IMF the results are suggestive of plasma penetration from the poleward edge of the cusp, combined with a substantial sunward convection, but no flows are observed at all at the dayside boundary with the plasma sheet. The comparison of the measured flow speed with the Alfvén speed suggests that the magnetosheath adjacent to the external boundary is more sub-Alfvénic, even for high magnetic latitudes, under northward IMF than under southward IMF. This result is consistent with the preference for the plasma depletion layer to develop under such conditions. The transverse plasma convection in the exterior cusp appears to be controlled by the IMF B_Y component as well; for dawnward (duskward) IMF orientations the convection is preferentially directed toward dusk (dawn). These results are interpreted as strong arguments in favor of the cusp being structured, at large scales, by the occurrence of magnetic reconnection at the high-latitude magnetopause for northward IMF and at the low-latitude magnetopause for southward IMF.

Citation: Lavraud, B., A. Fedorov, E. Budnik, M. F. Thomsen, A. Grigoriev, P. J. Cargill, M. W. Dunlop, H. Rème, I. Dandouras, and A. Balogh (2005), High-altitude cusp flow dependence on IMF orientation: A 3-year Cluster statistical study, *J. Geophys. Res.*, *110*, A02209, doi:10.1029/2004JA010804.

1. Introduction

[2] The low- and middle-altitude cusp regions of the Earth's magnetosphere have been widely studied in the past [*Newell et al.*, 1989; *Lockwood and Smith*, 1992; *Yamauchi et al.*, 1996]. However, the high-altitude cusp region was not explored extensively in the early days of space science, with the notable exception of the HEOS-2 spacecraft which undertook the first detailed investigations of this part of the magnetosphere [e.g., *Paschmann et al.*, 1976; *Haerendel et al.*, 1978]. More recently, major advances on the role of this key region, which is in direct interaction with the solar wind, have been provided by the Polar [*Russell*, 2000; *Fuselier et al.*, 2000a; *Onsager et al.*, 2001], Interball [*Savin et al.*, 1998; *Fedorov et al.*, 2000; *Dubinin et al.*, 2002], and four-spacecraft Cluster missions [*Lavraud et al.*, 2002; *Nykyri et al.*, 2003; *Cargill et al.*, 2004]. Much of this work has focused on analysis of individual crossings, but a few statistical studies of the high-altitude cusp region have been undertaken using data from the HEOS-2 [*Dunlop et al.*, 2000], Hawkeye [*Zhou and Russell*, 1997; *Eastman et al.*, 2000], Polar [*Tsyganenko and Russell*, 1999], and Interball [*Grigoriev et al.*, 1999; *Měrka et al.*, 2002] data sets.

[3] Because of its high-quality data and its suitable orbit the four-spacecraft Cluster mission is perfectly adapted for high-altitude cusp investigations and therefore for large-

[1]Space Science and Applications, Los Alamos National Laboratory, Los Alamos, New Mexico, USA.
[2]Centre d'Etude Spatiale des Rayonnements, Toulouse, France.
[3]Swedish Institute of Space Physics, Kiruna, Sweden.
[4]Blackett Laboratory, Imperial College, London, UK.
[5]Rutherford Appleton Laboratory, Didcot, UK.

0148-0227/05/2004JA010804

scale statistical studies. *Lavraud et al.* [2004a] presented the first results of the statistical distributions of the magnetic field and plasma parameters in this region using Cluster data organized by a specific spatial sampling method, which was first introduced by *Grigoriev et al.* [1999]. *Lavraud et al.* [2004a] showed the existence of the various boundaries surrounding the exterior cusp diamagnetic cavity and focused on the ensemble of properties observed in this region for all interplanetary magnetic field (IMF) conditions.

[4] The actual flow pattern of the exterior cusp region is poorly known. While the exterior cusp is expected to be largely convective for southward IMF conditions and subsequent low-latitude reconnection [*Vasyliunas*, 1995], the occurrence of lobe reconnection for northward IMF may rather lead to the presence of more stagnant plasma in this region [*Lavraud et al.*, 2002].

[5] The possible occurrence of continuous reconnection at the low-latitude magnetopause under southward IMF conditions is now generally accepted [*Gosling et al.*, 1982; *Phan et al.*, 2004]. For northward IMF, however, strong evidence for such a reconnection regime at high latitudes, tailward of the cusp, was only recently provided by the remote detection of the UV emissions of accelerated protons precipitating in the ionosphere [*Frey et al.*, 2003]. Indeed, gas-dynamic models of the magnetosheath predict that the flows are super-Alfvénic near the high-latitude magnetopause, therefore preventing any reconnected magnetic field line from moving sunward and participating in the cusp formation. *Fuselier et al.* [2000b] postulated that the presence of a plasma depletion layer (PDL) [*Zwan and Wolf*, 1976] may render the flows in this region sub-Alfvénic, as indeed indicated by recent satellite observations [*Avanov et al.*, 2001; *Phan et al.*, 2003; *Lavraud et al.*, 2004b].

[6] In the global survey by *Lavraud et al.* [2004a] (hereinafter referred to as paper 1), high-altitude cusp properties were studied statistically without consideration of specific IMF orientations. The present study particularly focuses on a separate investigation of flow characteristics in the region for different IMF clock angle (CA) intervals. We give statistical results, in the form of spatial distributions, of the flow properties as a function of the IMF orientation.

[7] Section 2 summarizes the sampling technique used for ordering the data in space, as well as the results of paper 1. In section 3 we show the characteristics of the various distributions and discuss those in terms of (1) the magnetic field configuration of the magnetosphere around the high-altitude cusp for southward and northward IMF orientations, (2) the large-scale plasma convection in the exterior cusp for southward and northward IMF cases, (3) the location of magnetosheath plasma entry for southward and northward IMF cases, (4) the eventual effects of the presence of a sub-Alfvénic plasma depletion layer under northward IMF conditions, and (5) the IMF B_Y control of the transverse flows in this region. Conclusions are finally drawn in section 4.

2. Instrumentation, Methodology, and Summary of Paper 1

2.1. Instrumentation and Orbits

[8] In the present study we make use of the Cluster ion and magnetic field data from the Cluster Ion Spectrometry (CIS) [*Rème et al.*, 2001] and FluxGate Magnetometer (FGM) [*Balogh et al.*, 2001] instruments. The ion data come from the Hot Ion Analyser which allows measurements of the full three-dimensional ion distribution functions and moments up to a resolution of ~4 s (spin). Solar wind measurements come from the ACE spacecraft. Propagation lag times are calculated for each crossing by using the measured solar wind velocity and spacecraft location and are further adjusted by visual inspection. Because of the sampling method, all data are averaged as described in section 2.3.

[9] During the 2001 and 2002 periods the Cluster interspacecraft separation was ~600 and ~100 km, respectively. Consequently, only the data from spacecraft 3 are used for these periods. In 2003, however, the interspacecraft distance was about ~1 R_E, and the data from both spacecraft 1 and 3 are used.

2.2. Coordinate Transformations

[10] The orbit sampling is based on a technique (cf. paper 1) that takes into account the actual lagged solar wind (IMF and dynamic pressure (P_{dyn})) and geomagnetic (D_{ST}) conditions, by use of a magnetospheric magnetic field [*Tsyganenko*, 1995, 1996] (*Tsyganenko* [1996] hereinafter referred to as T96) and magnetopause [*Shue et al.*, 1997] model. The technique fixes the positions of the cusp boundaries in accordance with these external conditions by modeling the effects of these parameters on the location of the cusp and magnetopause. The advantage of this method is to enable spatial distributions of the measurements for the ensemble of possible IMF orientations (see paper 1). For the present paper, however, we instead sort the data according to a selection of IMF clock angle ($\tan^{-1}(B_Y/B_Z)$ in GSM) intervals.

[11] The Cluster spacecraft orbits are sampled every 2 min and are transformed into a normalized frame of reference. The objective of this transformation is to organize the data in a given spatial plane, and thus we first need to fold the orbit points into the $(X, Z)_{SM}$ plane. The next step aims to take into account the cusp latitudinal displacement, based on the T96 magnetic field model and according to some reference solar wind and geomagnetic conditions. The last step consists of a radial adjustment of the orbit points to take into account the magnetopause displacement as a function of these conditions. The exact steps of this superposed analysis technique may be detailed as follows and are illustrated in Figure 1:

[12] 1. Each orbit point A (SM coordinates) is transformed into A′ through rotation about the X_{SM} axis into the $(X, Z)_{SM}$ plane (Figure 1a). The resulting upward axis is a radius; the distributions plane is called $(X, R)_{Norm}$.

[13] 2. The T96 magnetic field model is used to fix a reference frame for the following reference conditions: IMF = (0.0; 2.0; 0.0) nT, P_{dyn} = 2.5 nPa, and D_{ST} = −10.0 nT. These dynamic pressure and D_{ST} parameters are chosen as typical values. The duskward IMF orientation is used to avoid biasing the reference frame toward the equator (southward IMF) or the poles (northward IMF) [*Newell et al.*, 1989]. In the T96 model and for these conditions we identify the latitude of the separatrix between the last field line that is bent (or draped) toward the dayside and the first field line that extends back onto

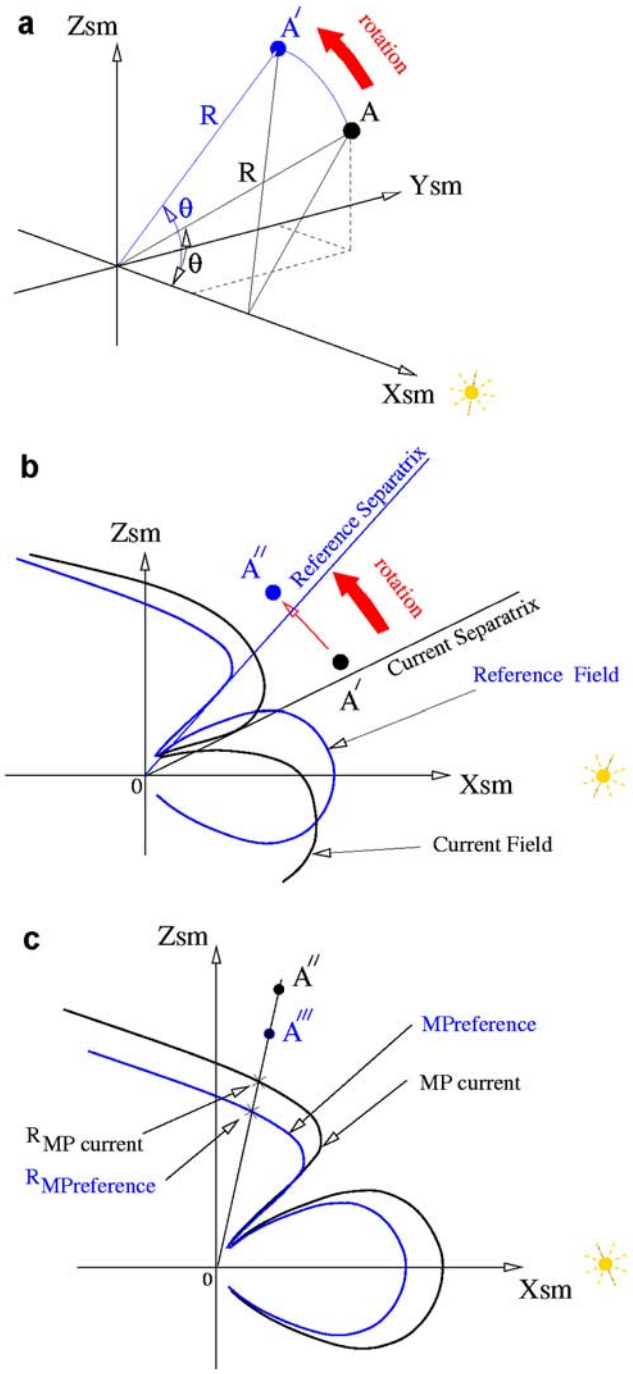

Figure 1. Representation of the various coordinate transformations: (a) rotation of all orbit points about the X_{SM} axis, which results in a projection into the $(X, Z)_{SM}$ plane, (b) rotation about the Y_{SM} axis as defined by the current separatrix angle (see text) by use of the T96 magnetic field model, and (c) radial scaling of the orbit points as a function of the reference magnetopause position for the actual solar wind conditions (model from *Shue et al.* [1997]).

the nightside. This latitude angle is used as the "reference" angle of the reference separatrix (Figure 1b).

[14] 3. Each orbit point A′ is then transformed as follows. The actual lagged solar wind conditions and geomagnetic activity levels are used in the T96 model. A new, "current" separatrix angle between the dayside and nightside field lines is then defined for these conditions. A′ is rotated about the Y_{SM} axis so that its angular separation from the reference separatrix is equal to the original separation between A′ and the current separatrix. This rotation allows normalization of the orbit point to the reference frame. The resulting orbit point is A″ (Figure 1b).

[15] 4. Finally, a radial adjustment is performed. By use of the *Shue et al.* [1997] magnetopause model we define a reference magnetopause location for the reference solar wind and geomagnetic conditions given above. We then scale radially the point A″ proportionally to the ratio of the reference magnetopause position to the one calculated for the actual external conditions. This final orbit point is A‴ (Figure 1c).

[16] These coordinate transformations are applied to all the Cluster orbits for which CIS, FGM, and ACE data are available. The magnetic field and flow vectors are also transformed according to the above steps. The spatial distributions are shown in the resulting normalized $(X, R)_{Norm}$ plane.

2.3. Orbit and Data Sampling

[17] Cluster CIS and FGM measurements are averaged over intervals of 2 min to match the orbit sampling. The interplanetary conditions are sampled for intervals of 10 min, and averages over these intervals are made. These values are thus used for five successive orbit samples. In the present survey we make use of 163 cusp passes.

[18] Only orbit points for which the radial direction forms an angle with the $(X, Z)_{SM}$ plane <25° have been used, so that encounters with the flank low-latitude boundary layer and plasma sheet are avoided. By using the technique described in section 2.2, we obtain spatial distributions of the data in a predefined grid of the $(X, R)_{Norm}$ plane by averaging the measurements coming from all the orbit points that fall into square bins of size 0.3 R_E. In the displays of the statistical properties in Figures 3–6, each square bin is presented as proportionally sized according to the amount of samples averaged but saturated at a maximum size of 0.3 R_E when more than 20 samples are averaged. In Figures 2–6 the T96 magnetic field configuration, for the reference conditions, is displayed as a background for guidance (black field lines).

2.4. Summary of Paper 1

[19] In Figure 2 of paper 1 the distributions of the solar wind and geomagnetic parameters for the entire data set were presented. In particular, it was shown that the coverage of the data set in terms of IMF clock angle ($\tan^{-1}(B_Y/B_Z)$ in GSM) was complete, with a large number of samples for any given direction. The use of selected IMF clock angle intervals in the present survey is therefore not a priori biased by a lack of statistics (see details in paper 1).

[20] The global properties of the high-altitude cusp have been discussed in paper 1 for distributions using all IMF directions. The results of that paper may be summarized as follows. (1) The magnetic field distribution clearly showed the presence of an intermediate region between the magnetosheath and the magnetosphere: the exterior cusp. (2) This region was characterized by the presence of

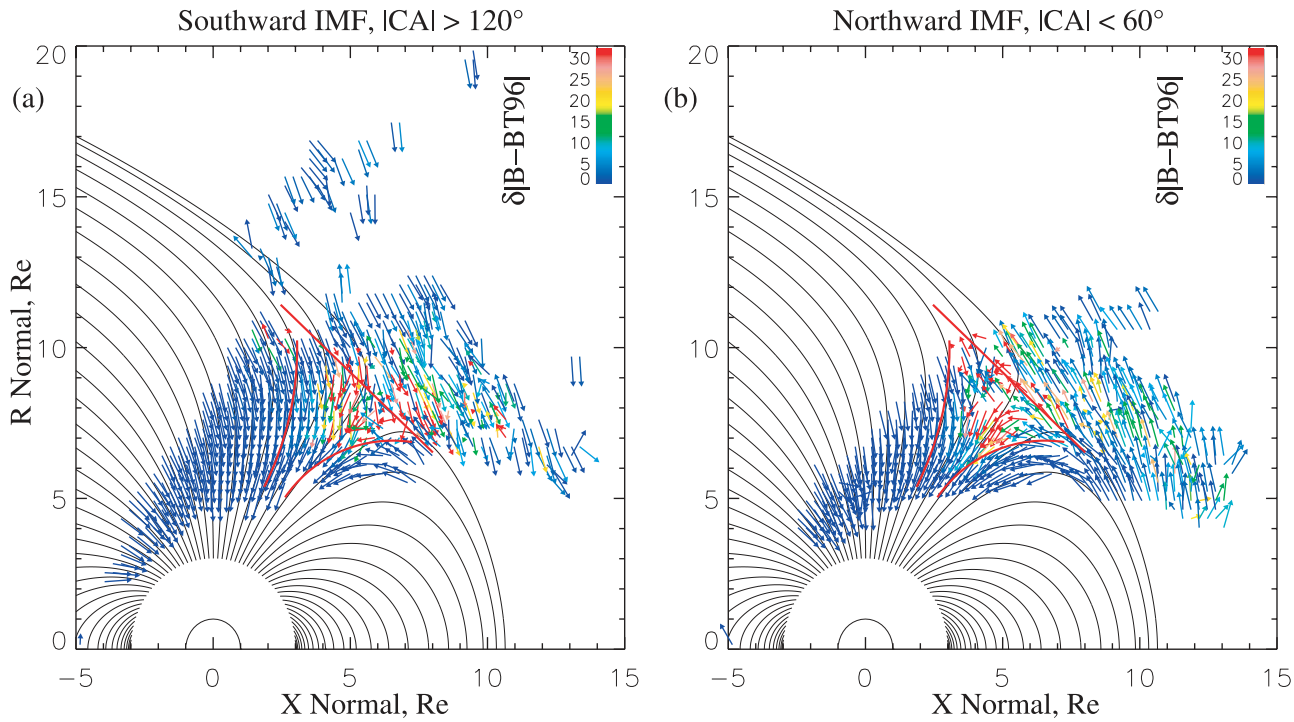

Figure 2. Spatial distributions of the magnetic field vectors measured by FGM in the high-latitude, high-altitude northern magnetosphere for (a) southward IMF (CA = $\tan^{-1}(B_Y/B_Z)$ in GSM coordinates; |CA| > 120°) and (b) northward IMF (|CA| < 60°). Magnetic field vectors correspond to a projection using the transformations described in section 2. Size of each vector is |**B**| magnitude in logarithmic scale. Color of the vectors corresponds to the deviation of the measured **B** from the model **B** T96: ($\langle|\mathbf{B}_{meas} - \mathbf{B}_{T96}|\rangle$). Corresponding color scale is given at the top right-hand corner of each distribution. Background magnetic field lines have been computed from the T96 model for the reference conditions.

dense plasma of magnetosheath origin, and a comparison with the T96 magnetic field model showed that the exterior cusp is diamagnetic in nature. (3) The spatial distributions of most parameters demonstrated that three distinct boundaries with the lobes, the dayside plasma sheet, and the magnetosheath surround the exterior cusp. (4) The external boundary with the magnetosheath has a sharp bulk velocity gradient as well as a density decrease and temperature increase as one goes from the magnetosheath to the exterior cusp. (5) While the two inner boundaries formed a funnel, the external boundary showed no obvious indentation. (6) The plasma and magnetic pressure distributions suggested that the exterior cusp is in equilibrium with its surroundings in a statistical sense. (7) Finally, a preliminary analysis of the bulk flow distributions suggested that the exterior cusp may be stagnant under northward IMF but convective under southward IMF. In the present paper we focus on the detailed characteristics of the flows in the high-altitude cusp for various IMF clock angle intervals.

3. Results and Discussion

[21] In this section we show and discuss the results of the technique, when applied to Cluster CIS and FGM measurements for selected IMF clock angle intervals. We interpret the distributions of the plasma flows in the context of solar wind plasma penetration, convection, and transport into the cusp and magnetosphere.

[22] All the figures presented in this paper show spatial distributions of the plasma and field parameters in the high-altitude and high-latitude regions of the northern magnetosphere. In all the plots the high-altitude exterior cusp region is shown to be bounded by three distinct boundaries indicated by red lines. These boundaries were defined in paper 1 by use of the bulk velocity, density, and temperature distributions calculated for all IMF conditions. Here these lines are only meant to serve as guides. They separate the exterior cusp from the lobes (or plasma mantle) on the poleward side from the dayside plasma sheet on the equatorward side and from the magnetosheath outward.

3.1. Magnetic Field Configuration

[23] We present the magnetic configuration of the whole region in the form of averaged magnetic field vectors measured by FGM in Figures 2a and 2b (normalized coordinates) for southward (|CA| > 120°) and northward (|CA| < 60°) IMF orientations, respectively. The magnetic field vectors are scaled logarithmically to their magnitude, and their color coding represents the deviation of the measurements from the T96 model magnetic field (see caption for details). Because the T96 model sets the magnetosheath field to the actual IMF values (B_Y and B_Z, but B_X = 0 nT), the deviations (colors) observed in the magnetosheath should be given no particular meaning (see also paper 1).

[24] From both the vector orientations and the deviations from T96, one can see that the location of the equatorward

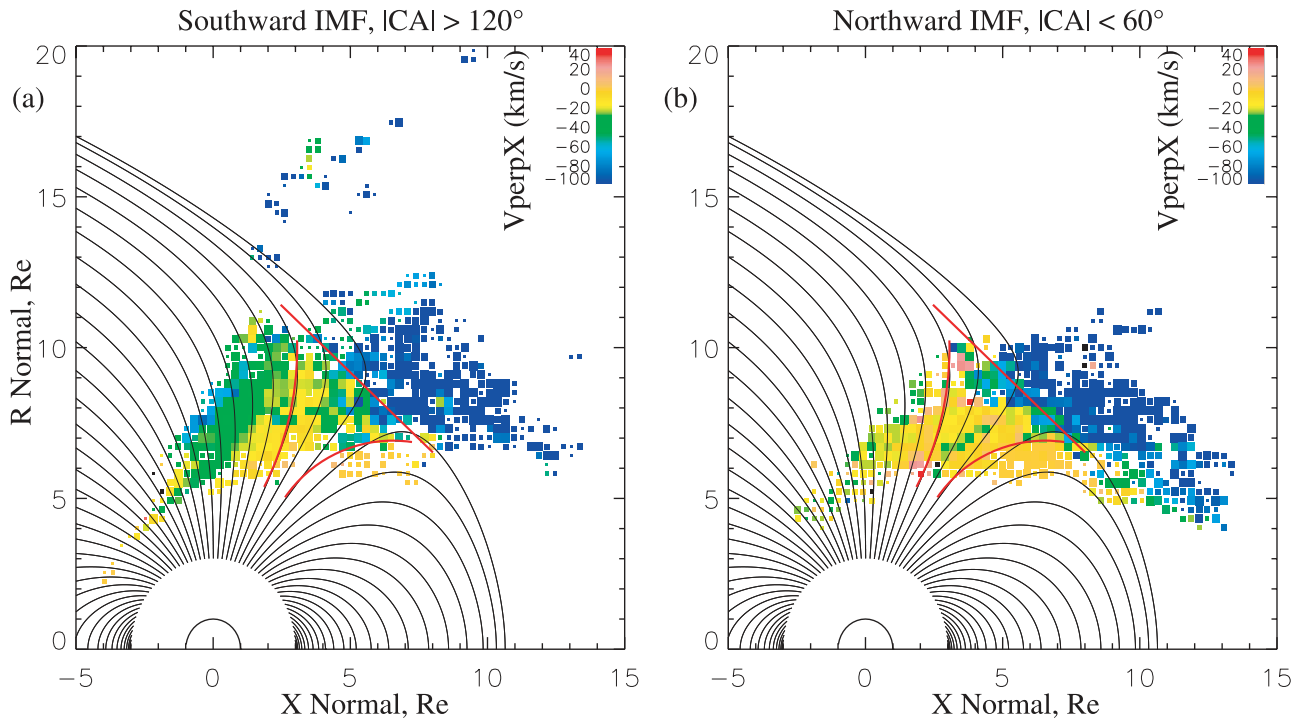

Figure 3. Spatial distributions of the X component of the convection (perpendicular to the magnetic field, V_{perpX}) velocity in the high-altitude cusp and surrounding regions for (a) southward ($|CA| > 120°$) and (b) northward ($|CA| < 60°$) IMF. Velocity vectors correspond to a projection using the transformations described in section 2. Observations have been collected and then averaged over spatial bins of 0.3 R_E. Size of the displayed color squares is proportional to the number of samples accumulated in the appropriate spatial bin. Their size is saturated at 0.3 R_E when the number of samples exceeds 20. Color of the bins indicates the magnitude of V_{perpX}. Corresponding color scale is shown in the top right-hand corner of each distribution, with blue (red) color indicating tailward (sunward) convection. Background magnetic field lines have been computed from the T96 model for the reference conditions.

boundary of the exterior cusp is independent of the IMF direction. In both IMF cases this boundary manifests itself by large deviations from the T96 magnetic field model. This fact proves that the coordinate transformation technique used here allows an adequate epoch superposition for each IMF orientation. In between the three boundaries the exterior cusp shows clear deviations from the T96 model. This vacuum model does not make use of diamagnetic current systems and therefore does not reproduce the diamagnetic nature of this region. Further discussion on that topic may be found in paper 1.

[25] A second interesting feature is the relatively weak magnetic deviation (measured against the model) observed near the poleward edge of the exterior cusp. Although both density and temperature may on average be nonnegligible in this region (see paper 1), the magnetic field magnitude there is higher than that in the outermost part of the cusp. This probably results in a lower plasma Beta and hence a lower diamagnetic effect on the lobe/plasma mantle field lines.

[26] The magnetosheath magnetic field configuration near the outer boundary is consistent with that expected from the selected IMF orientation in both Figures 2a and 2b. It is worth noting that the configuration of the whole region appears compatible with an open magnetosphere where the topology results from low- and high-latitude reconnection for southward and northward IMF directions, respectively. While the southward IMF case displays some evidence for a possible normal component of the field across the boundary, the northward IMF case shows a more draped magnetic field topology close to the outer boundary.

3.2. Plasma Convection

[27] Figures 3a and 3b show the spatial distributions of the X component of plasma convection (V_{perpX} in normalized coordinates) for southward and northward IMF, respectively. In both IMF cases the magnetosheath always shows a large tailward convection on average, which is expected. As also expected, the dayside plasma sheet, equatorward of the cusp, shows basically no flows ($V_{perpX} \sim 0$ km/s).

[28] Within the exterior cusp and adjacent magnetospheric regions, clear differences are observed between the southward and northward IMF cases. A clear tailward convection (all $V_{perpX} < -20$ km/s) is observed in the region $X_{Norm} = 5–7$ and $R_{Norm} = 6–9$ R_E near the boundary with the dayside plasma sheet for southward IMF. The tailward convection is large compared to that of the adjacent plasma sheet. It is observed to decrease with increasing latitude into the plasma mantle and lobe regions, but it always keeps a tailward orientation.

[29] For the case of northward IMF the distribution looks very different. No particular feature appears near the equatorward cusp boundary. The average tailward convection speed in most of the cusp region is lower than 10 km/s, so that the region may be considered as stagnant for the given

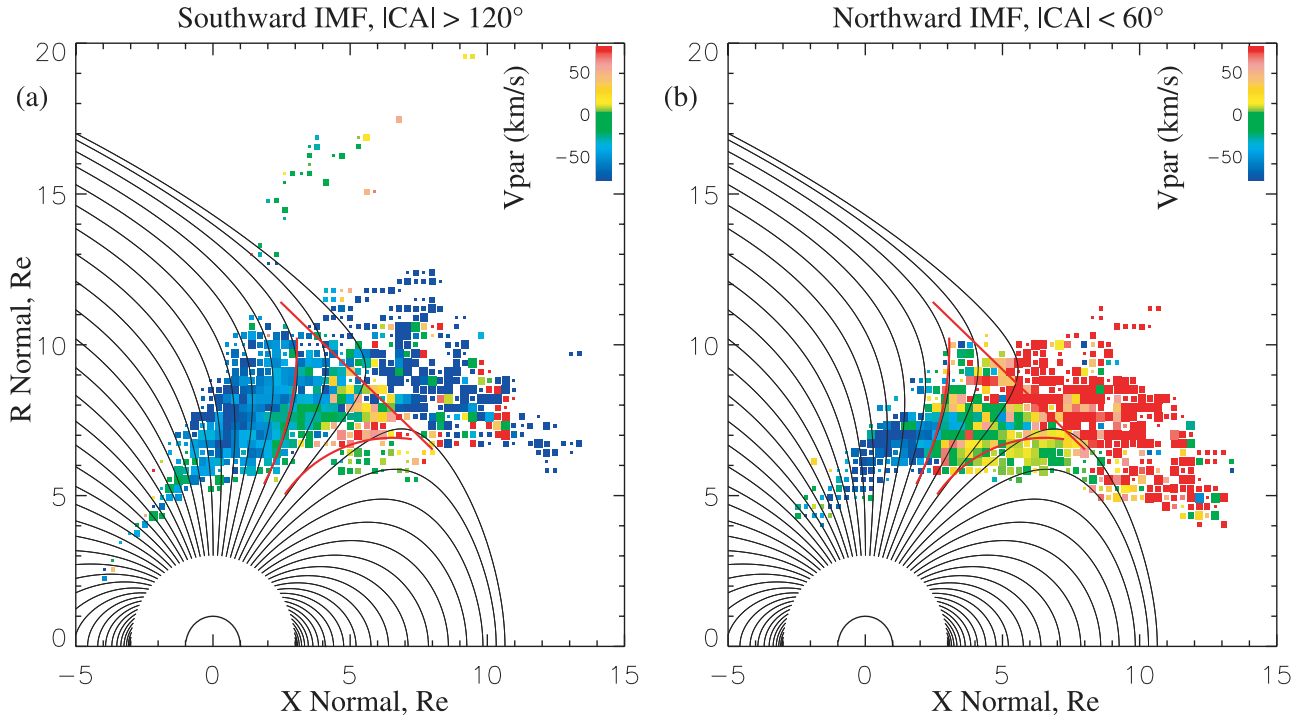

Figure 4. Spatial distributions of the field-aligned ion flows observed in the region for (a) southward (|CA| > 120°) and (b) northward (|CA| < 60°) IMF. Field-aligned velocity magnitude is color coded. Appropriate color scale is shown in the top right-hand corner of each distribution. Red color indicates field-aligned flow. See Figure 3 caption and text for details.

northward IMF conditions. Furthermore, a small sunward convection ($V_{perpX} > 0$, indicated by red in the color scale) is clearly seen at the poleward edge of the cusp, near X_{Norm} = 1–3 and R_{Norm} = 6–9 R_E.

[30] The enhanced tailward convection at the equatorward edge of the cusp when the IMF is southward as well as the signature of sunward convection near the poleward edge of the cusp for northward IMF are consistent with the hypothesis that the reconnection site moves from the low-latitude magnetopause to the high-latitude (lobe) magnetopause if the IMF direction turns from southward to northward. Another proof for this hypothesis would be the observation of an asymmetry in the field-aligned plasma flows, given the expected different location of the reconnection site for each IMF orientation.

3.3. Field-Aligned Plasma Flow

[31] Figures 4a and 4b show the spatial distributions of the field-aligned ion flows for southward and northward IMF, respectively. In the case of southward IMF, large downward field-aligned flows (red color) are clearly observed at the equatorward boundary of the cusp. This layer is thus collocated with the region of large tailward convection. The combination of plasma injection at this location and of the subsequent tailward large-scale convection in the region is compatible with the generally accepted cusp model for southward IMF [*Lockwood and Smith*, 1994]. In this model the magnetic field lines adjacent to the equatorward cusp boundary are magnetically connected to the open magnetopause at low latitudes. Magnetosheath plasma enters the magnetopause boundary layer and populates those field lines. The large speeds are the result of the large magnetic shear at the low-latitude magnetopause for such IMF orientations, and the large tailward convection renders the flows clearly detectable due to the velocity filter effect.

[32] By contrast, no such plasma precipitation is observed near the plasma sheet boundary in the northward IMF case. Rather, some indication of downward field-aligned flows at high latitudes is observed near X_{Norm} = 2–4 and R_{Norm} = 6–9 R_E. Although these look fainter (and will merit further inspection when more Cluster passes are available), they are correlated with the presence of the sunward convection observed near the poleward cusp boundary reported in section 3.2. These distributions therefore suggest the occurrence of reconnection at the high-latitude lobe magnetopause. In contrast to the low-latitude reconnection, which generally covers a wide longitudinal region, the plasma precipitation from high-latitude reconnection is confined to a small spatial region [*Frey et al.*, 2003]. This may explain the weaker evidence for sunward convection and high-latitude field-aligned flows in our statistics for northward IMF.

3.4. Alfvén Mach Number

[33] Figures 5a and 5b display the spatial distributions of the Alfvén Mach number ($M_A = |V_{ions}|/|V_{Alfvén}|$) in the high-altitude cusp region for southward and northward IMF conditions. On average, it is seen that the Mach number is low ($M_A < 1$) inside the magnetosphere and in the exterior cusp region, for both IMF conditions. Outside the external boundary the magnetosheath flow is overall super-Alfvénic for both IMF cases, but a specific feature appears for northward IMF in Figure 5b.

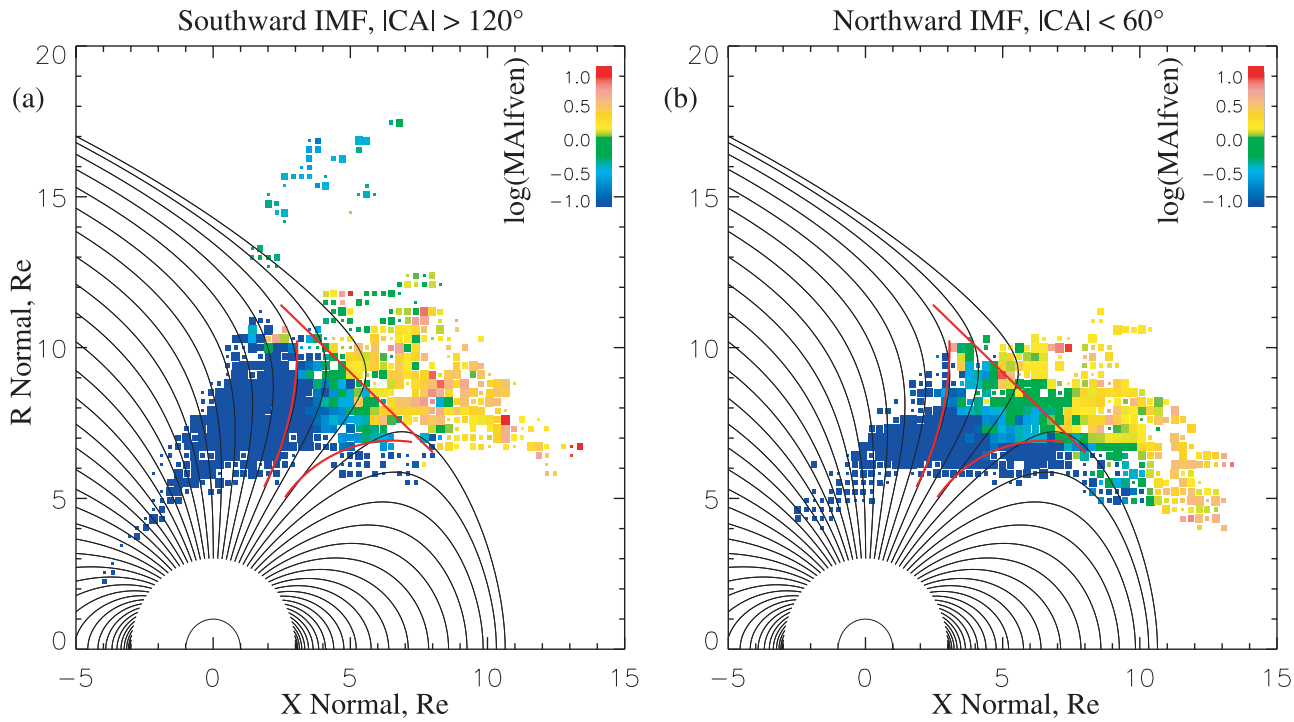

Figure 5. Spatial distributions of the Alfvén Mach number are shown for (a) southward (|CA| > 120°) and (b) northward (|CA| < 60°) IMF. Color of the bins indicates the logarithm of the Alfvén Mach number. Corresponding color scale is shown in the top right-hand corner of each distribution. Green color corresponds to the transition from super- to sub-Alfvénic flows. See Figure 3 caption and text for details.

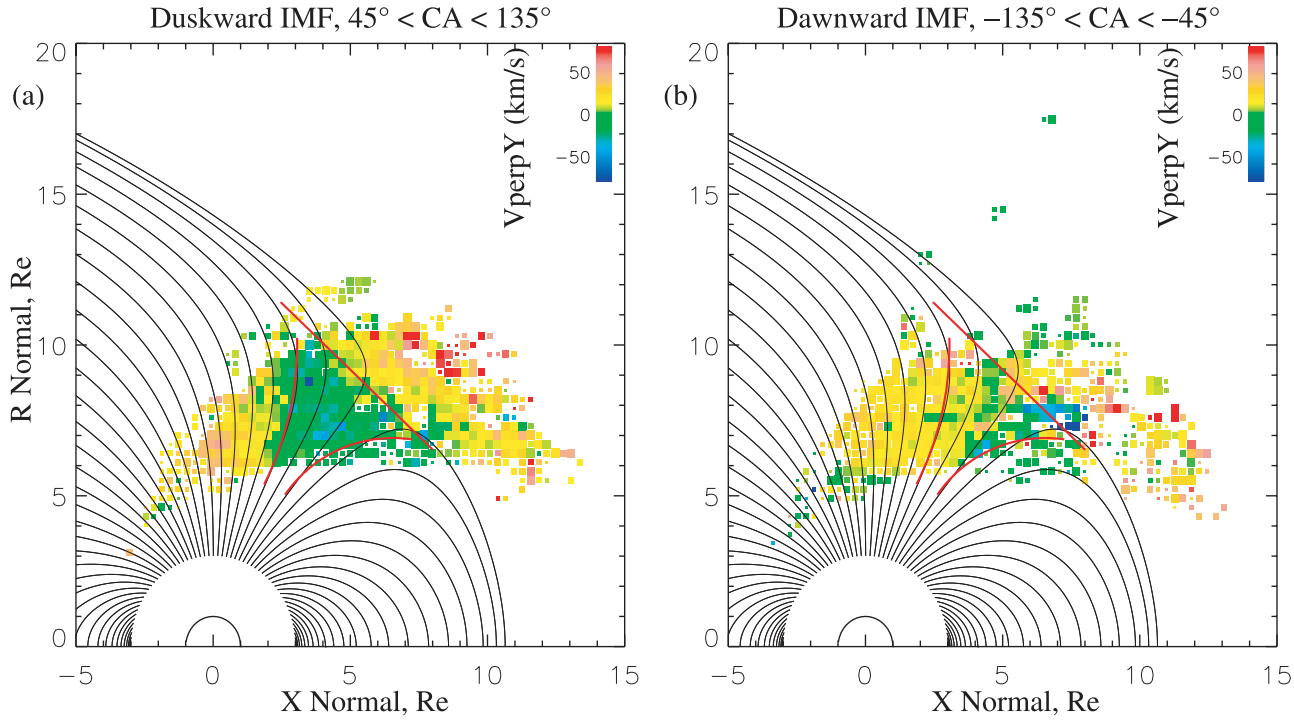

Figure 6. Spatial distributions of the Y component of the convection (perpendicular to the magnetic field) velocity (V_{perpY}) for (a) duskward (45° < CA < 135°) and (b) dawnward (−135° < CA < −45°) IMF. Color of the bins indicates the magnitude of V_{perpY}. Dark green to blue colors indicate dawnward flows, while yellow to red colors correspond to duskward flows. See Figure 3 caption and text for details.

[34] The region just outside the external boundary is clearly characterized by super-Alfvénic flows (orange or red) under southward IMF. In contrast, for northward IMF, the flows are close to $M_A = 1$ or less (greener) within a layer just adjacent to the outer boundary. On average, the transition from super- to sub-Alfvénic flows seems to be located at larger radial distances for northward IMF, apparently well inside the magnetosheath. This characteristic is further supported by the examination of the velocity distributions of Figures 3 and 4. In these latter figures the flows (both parallel and perpendicular) are large and characteristic of the magnetosheath outside the outer boundary (red line) for both the southward and northward IMF cases.

[35] This layer is possibly due to the presence of PDLs in this region. Such layers are the result of magnetic field piling up on the front side magnetosphere, combined with plasma depletion by flowing along the draped magnetosheath field lines [*Zwan and Wolf*, 1976]. While a PDL may easily form and be observed under northward IMF, even at high magnetic latitudes, the magnetic pileup process is partially suppressed for southward IMF when low-latitude reconnection takes place [*Fuselier et al.*, 2000b]. A PDL is thus characterized by an increased magnetic field magnitude and a decreased density, thus eventually rendering the flows in this region sub-Alfvénic, as observed in our distribution for northward IMF. This finding is compatible with the possible stability of the high-latitude reconnection site [*Fuselier et al.*, 2000b].

3.5. Transverse Plasma Flows

[36] Figures 6a and 6b display the spatial distributions of the Y component of the convection (V_{perpY}, perpendicular velocity in normalized coordinates) for IMF orientations toward dusk ($45° < CA < 135°$) and dawn ($-135° < CA < -45°$), respectively. An obvious dawn-dusk asymmetry is seen close to the poleward boundary in the exterior cusp. The convection is on average directed dawnward for duskward IMF while it is directed duskward for dawnward IMF. Such a behavior (convection opposite to the IMF direction) is that expected from the tangential stress exerted on a reconnected field line in the Northern Hemisphere. This property is compatible with case study observations at both the low- [*Gosling et al.*, 1990] and high-latitude magnetopause [*Gosling et al.*, 1991]. However, it is noted that, while this behavior is well pronounced in the case of duskward IMF, the dawnward IMF case shows a more complex structure, in particular near the equatorward boundary.

4. Conclusion

[37] We have presented statistical spatial distributions of the magnetic field configuration and plasma flows in the high-altitude cusp and surrounding regions. Here we summarize our findings and their implications.

[38] For southward IMF the large downward flows observed at the equatorward edge of the high-altitude cusp are correlated with large tailward convection in our distributions. By contrast, these flows are absent at this location for northward IMF. Rather, the flow distributions for northward IMF conditions are suggestive of plasma penetration taking place at the poleward edge of the cusp, combined with a sunward convection there. These results indicate that the exterior cusp flow structure is compatible with the preferential presence of reconnection at low latitudes for southward IMF and at high latitudes in the lobes for northward IMF.

[39] When reconnection occurs at high latitudes, the rotational discontinuity and thus the reconnected field lines propagate opposite to the external magnetosheath flow, contrary to the case of low-latitude reconnection and tailward convection (where the propagation is in the sense of the magnetosheath flow). As a result the convection patterns are opposite in terms of direction between the two IMF cases, but the flows are much lower in terms of magnitude in the northward IMF case, leading to the presence of stagnant plasma in the exterior cusp [*Lavraud et al.*, 2002, 2004b]. This property is shown statistically in the present study.

[40] This scenario, in the context of possible steady reconnection in the lobes [*Frey et al.*, 2003], may only be sustained by the presence of sub-Alfvénic flows in the magnetosheath just adjacent to the external boundary and possibly at the lobe reconnection site under northward IMF. This possibility had been suggested by *Fuselier et al.* [2000b], and observational evidence was presented by *Avanov et al.* [2001], *Phan et al.* [2003], and *Lavraud et al.* [2004b]. Our statistics have shown the possible recurrent presence of a sub-Alfvénic PDL at high magnetic latitudes. However, Cluster only passes infrequently through the high-latitude magnetopause [*Phan et al.*, 2003]. The number of samples near the possible lobe reconnection site is thus low, and we cannot yet address the possibility of a permanent sub-Alfvénic flow in the magnetosheath near this region for northward IMF.

[41] These findings suggest that reconnection determines the large-scale structure of the high-altitude cusp. This is further supported by the clear dependence of the transverse convection in the region on the IMF B_Y component (Figure 6).

[42] From these global characteristics it is seen that the penetration location and subsequent convection of the plasma in the high-altitude cusp region are substantially different for the particular cases of southward and northward IMF directions. For southward IMF and low-latitude reconnection the solar wind plasma enters the cusp from its equatorward edge. It is convected tailward and therefore transported into the plasma mantle and eventually into the tail regions of the magnetosphere. For northward IMF the global dynamics are different. The solar wind plasma enters the cusp from its poleward side. It is decelerated (in terms of convection) upon entry and forms a rather stagnant region made of cold (compared to the dayside plasma sheet), dense plasma. Therefore, in the eventuality of reconnection occurring at the lobes of both hemispheres during northward IMF conditions, the exterior cusp may be viewed as a potential plasma source for the low-latitude boundary layers and the cold, dense plasma sheet.

[43] **Acknowledgments.** The authors are grateful to the CIS and FGM teams for their incomparable work in data processing. We thank the ACE MFI and SWEPAM instruments teams and the CDAWeb for providing the ACE data. P.C. acknowledges support from PPARC through a Senior Research Fellowship. Work at Los Alamos was conducted under the auspices of the U.S. Department of Energy, with support from the NASA Cluster program.

[44] Lou-Chuang Lee thanks Timothy Eastman and Harald Frey for their assistance in evaluating this paper.

References

Avanov, L. A., V. N. Smirnov, J. H. Waite Jr., S. A. Fuselier, and O. L. Vaisberg (2001), High-latitude magnetic reconnection in sub-Alfvénic flow: Interball tail observations on May 29, 1996, *J. Geophys. Res.*, *106*(A12), 29,491–29,502.

Balogh, A., et al. (2001), The Cluster magnetic field investigation: Overview of in-flight performance and initial results, *Ann. Geophys.*, *19*(10–12), 1207–1217.

Cargill, P. J., M. W. Dunlop, B. Lavraud, R. C. Elphic, D. L. Holland, K. Nykyri, A. Balogh, I. Dandouras, and H. Rème (2004), CLUSTER encounters with the high altitude cusp: Boundary structure and magnetic field depletions, *Ann. Geophys.*, *22*(5), 1739–1754.

Dubinin, E., et al. (2002), Polar-Interball coordinated observations of plasma and magnetic field characteristics in the regions of the northern and southern distant cusps, *J. Geophys. Res.*, *107*(A5), 1053, doi:10.1029/2001JA900068.

Dunlop, M. W., P. J. Cargill, T. J. Stubbs, and P. Wooliams (2000), The high-altitude cusps: HEOS-2, *J. Geophys. Res.*, *105*(A12), 27,509–27,517.

Eastman, T. E., S. A. Boardsen, S.-H. Chen, and S. F. Fung (2000), Configuration of high-latitude and high-altitude boundary layers, *J. Geophys. Res.*, *105*(A10), 23,221–23,238.

Fedorov, A., E. Dubinin, P. Song, E. Budnik, P. Larson, and J.-A. Sauvaud (2000), Characteristics of the exterior cusp for steady southward IMF: Interball observations, *J. Geophys. Res.*, *105*(A7), 15,945–15,957.

Frey, H. U., T. D. Phan, S. A. Fuselier, and S. B. Mende (2003), Continuous magnetic reconnection at Earth's magnetopause, *Nature*, *426*(6966), 533–537.

Fuselier, S. A., K. J. Trattner, and S. M. Petrinec (2000a), Cusp observations of high- and low-latitude reconnection for northward IMF, *J. Geophys. Res.*, *105*(A1), 253–266.

Fuselier, S. A., S. M. Petrinec, and K. J. Trattner (2000b), Stability of the high-latitude reconnection site for steady northward IMF, *Geophys. Res. Lett.*, *27*(4), 473–476.

Gosling, J. T., J. R. Asbridge, S. J. Bame, W. C. Feldman, G. Paschmann, N. Sckopke, and C. T. Russell (1982), Evidence for quasi-stationary reconnection at the dayside magnetopause, *J. Geophys. Res.*, *87*(A4), 2147–2158.

Gosling, J. T., M. F. Thomsen, S. J. Bame, R. C. Elphic, and C. T. Russell (1990), Plasma flow reversals at the dayside magnetopause and the origin of asymmetric polar cap convection, *J. Geophys. Res.*, *95*(A6), 8073–8084.

Gosling, J. T., M. F. Thomsen, S. J. Bame, R. C. Elphic, and C. T. Russell (1991), Observations of reconnection of interplanetary and lobe magnetic field lines at high-latitude magnetopause, *J. Geophys. Res.*, *96*(A8), 14,097–14,106.

Grigoriev, A., A. Fedorov, E. Budnik, and N. S. Nikolaeva (1999), Magnetospheric magnetic field in the outer cusp region: Comparison of measurements obtained from the INTERBALL-1 satellite and from the T96 model, *Cosmic Res., Engl. Transl.*, *37*, 594–599.

Haerendel, G., G. Paschmann, N. Sckopke, H. Rosenbauer, and P. C. Hedgecock (1978), The frontside boundary layer of the magnetosphere and the problem of reconnection, *J. Geophys. Res.*, *83*(A7), 3195–3216.

Lavraud, B., et al. (2002), Cluster observations of the exterior cusp and its surrounding boundaries under northward IMF, *Geophys. Res. Lett.*, *29*(20), 1995, doi:10.1029/2002GL015464.

Lavraud, B., A. Fedorov, E. Budnik, A. Grigoriev, P. J. Cargill, M. W. Dunlop, H. Rème, I. Dandouras, and A. Balogh (2004a), Cluster survey of the high-altitude cusp properties: A three-year statistical study, *Ann. Geophys.*, *22*(8), 3009–3019.

Lavraud, B., et al. (2004b), The exterior cusp and its boundary with the magnetosheath: Cluster multi-event analysis, *Ann. Geophys.*, *22*(8), 3039–3054.

Lockwood, M., and M. F. Smith (1992), The variation of reconnection rate at the dayside magnetopause and cusp ion precipitation, *J. Geophys. Res.*, *97*(A10), 14,841–14,847.

Lockwood, M., and M. F. Smith (1994), Low and middle altitude cusp particle signatures for general magnetopause reconnection rate variations: 1. Theory, *J. Geophys. Res.*, *99*(A5), 8531–8553.

Měrka, J., J. Šafránková, and Z. Němeček (2002), Cusp-like plasma in high altitudes: A statistical study of the width and location of the cusp from Magion-4, *Ann. Geophys.*, *20*(3), 311–320.

Newell, P. T., C. I. Meng, D. G. Sibeck, and P. Lepping (1989), Some low-altitude cusp dependencies on the interplanetary magnetic field, *J. Geophys. Res.*, *94*(A7), 8921–8927.

Nykyri, K., P. J. Cargill, E. A. Lucek, T. S. Horbury, A. Balogh, B. Lavraud, I. Dandouras, and H. Rème (2003), Ion cyclotron waves in the high altitude cusp: CLUSTER observations at varying spacecraft separations, *Geophys. Res. Lett.*, *30*(24), 2263, doi:10.1029/2003GL018594.

Onsager, T. G., J. D. Scudder, M. Lockwood, and C. T. Russell (2001), Reconnection at the high-latitude magnetopause during northward interplanetary magnetic field conditions, *J. Geophys. Res.*, *106*(A11), 25,467–25,488.

Paschmann, G., G. Haerendel, N. Sckopke, H. Rosenbauer, and P. C. Hedgecock (1976), Plasma and magnetic field characteristics of the distant polar cusp near local noon: The entry layer, *J. Geophys. Res.*, *81*(16), 2883–2899.

Phan, T. D., et al. (2003), Simultaneous Cluster and IMAGE observations of cusp reconnection and auroral proton spot for northward IMF, *Geophys. Res. Lett.*, *30*(10), 1509, doi:10.1029/2003GL016885.

Phan, T. D., et al. (2004), Cluster observations of continuous reconnection at the magnetopause under steady interplanetary magnetic field conditions, *Ann. Geophys.*, *22*(7), 2355–2367.

Rème, H., et al. (2001), First multispacecraft ion measurements in and near the Earth's magnetosphere with the identical CLUSTER Ion Spectrometry (CIS) Experiment, *Ann. Geophys.*, *19*(10–12), 1303–1354.

Russell, C. T. (2000), POLAR eyes the cusp, *Eur. Space Agency Spec. Publ., ESA SP-449*, 47–55.

Savin, S. P., et al. (1998), The cusp/magnetosheath interface on May 29, 1996: Interball 1 and Polar observations, *Geophys. Res. Lett.*, *25*(15), 2963–2966.

Shue, J.-H., J. K. Chao, H. C. Fu, C. T. Russell, P. Song, K. K. Khurana, and H. J. Singer (1997), A new functional form to study the solar wind control of the magnetopause size and shape, *J. Geophys. Res.*, *102*(A5), 9497–9511.

Tsyganenko, N. A. (1995), Modeling the Earth's magnetospheric magnetic field confined within a realistic magnetopause, *J. Geophys. Res.*, *100*(A4), 5599–5612.

Tsyganenko, N. A. (1996), Effects of the solar wind conditions on the global magnetospheric configuration as deduced from data-based field models, *Eur. Space Agency Spec. Publ., ESA SP-389*, 181–186.

Tsyganenko, N. A., and C. T. Russell (1999), Magnetic signatures of the distant polar cusps: Observations from Polar and quantitative modeling, *J. Geophys. Res.*, *104*(A11), 24,939–24,955.

Vasyliunas, V. M. (1995), Multi-branch model of the open magnetopause, *Geophys. Res. Lett.*, *22*(9), 1245–1247.

Yamauchi, M., et al. (1996), Dynamic response of the cusp morphology to the solar wind: A case study during passage of the solar wind plasma cloud on February 21, 1994, *J. Geophys. Res.*, *101*(A11), 24,675–24,687.

Zhou, X.-W., and C. T. Russell (1997), The location of the high-latitude polar cusp and the shape of the surrounding magnetopause, *J. Geophys. Res.*, *102*(A1), 105–110.

Zwan, B. J., and R. A. Wolf (1976), Depletion of solar wind plasma near a planetary boundary, *J. Geophys. Res.*, *81*(10), 1636–1648.

A. Balogh and P. J. Cargill, Blackett Laboratory, Imperial College, Exhibition Road, London SW7 2AZ, UK.

E. Budnik, I. Dandouras, A. Fedorov, and H. Rème, Centre d'Etude Spatiale des Rayonnements, 9 ave du Colonel Roche, F-31028, Toulouse cedex 4, France.

M. W. Dunlop, Rutherford Appleton Laboratory, Chilton, Didcot, Oxon OX11 0QXUK, UK.

A. Grigoriev, Swedish Institute of Space Physics, Box 812, SE-981 28 Kiruna, Sweden.

B. Lavraud and M. F. Thomsen, Space Science and Applications, Los Alamos National Laboratory, P.O. Box 1663, MS D466, Los Alamos, NM 87545, USA. (lavraud@lanl.gov)